

# AREAL SOLENOID, DIPOLE AND STEERING MAGNETS DESIGN AND PERFORMANCE

A. Tsakanian<sup>#</sup>, B. Grigoryan, A. Gevorgyan, V. Khachatryan, H. Gagyan, T. Mkrtchyan, M. Manukyan, S. Nagdalyan, A. Simonyan, V. Vardanyan, CANDLE SRI, Yerevan, Armenia

## Abstract

The AREAL solenoid, dipole and corrector magnets design, simulations and performance are presented. A solenoid magnet will be used for focusing the low energy ( $E \sim 5$  MeV) electron beam after RF gun as well as in the beam diagnostic section. The dipole magnet is part of the spectrometer for beam energy spread measurements. An Iron-free corrector magnet design allows independent horizontal and vertical beam steering. The design optimization and magnetic field calculations are performed using CST Studio Suite. A good agreement between measurements and simulations is obtained.

## INTRODUCTION

The AREAL test facility [1] is the laser driven RF photogun linear accelerator for generation of ultrashort electron bunches with small beam emittance in the energy range of 5-20 MeV. The first stage of the facility is aimed to obtain a 5 MeV energy electrons beam with bunch duration of 0.4-2 psec, the normalized emittance of 0.3 mm-mrad and bunch charge up to 200 pC. The magnetic system of the facility is an important part of the facility in order to provide the high performance of the electron beam and the main beam parameters measurements. This report presents the main design considerations for the dipole, solenoid and corrector magnets. The magnets design, simulation and optimization have been performed using the CST Studio Suite software [2]. The simulation results are compared with the measurements performed in the newly established Magnetic Measurement Bench station.

## DIPOLE MAGNET

As a part of AREAL spectrometer for energy and energy spread measurements, a dipole magnet was designed, fabricated and tested at the CANDLE Synchrotron Research Institute. The energy range of the electron beam is 2-5 MeV which is achieved just after the RF gun. The magnet design and geometry optimization are resulted on 12cm x 12cm square poles with gap of 4cm and yoke size of 8cmx6cm. In the simulations Steel-1008 material was used which properties are close to the measured steel used in magnet fabrication. The magnet consists of two coils with 500 windings each. In the field measurements the magnet-probe alignment  $<100\mu\text{m}$  was reached.

<sup>#</sup>tsakanian@asls.candle.am

Figure 2 presents the simulated and measured bending magnetic field distributions along the pole symmetry horizontal axes which are in good agreement.

Figure 3 presents simulated and measured bending field distributions along the electron 90° bend trajectory and measured field consistency with simulation results.

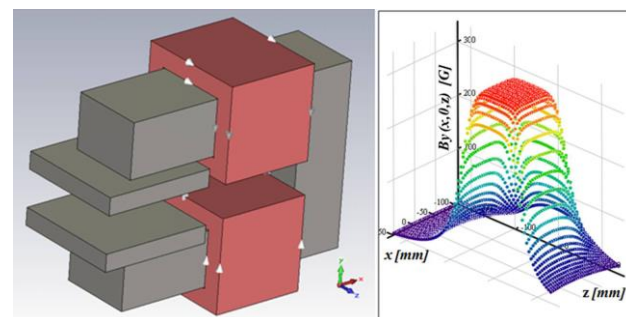


Figure 1: AREAL dipole magnet design and measured field map of bending field component.

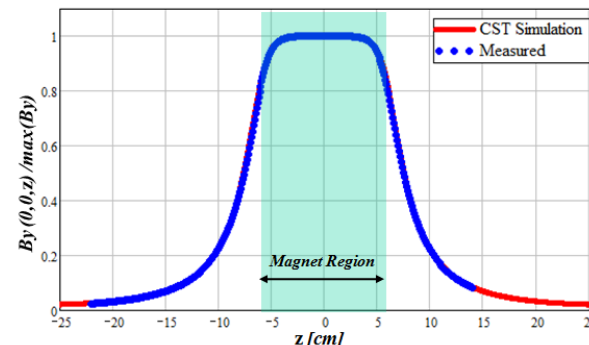
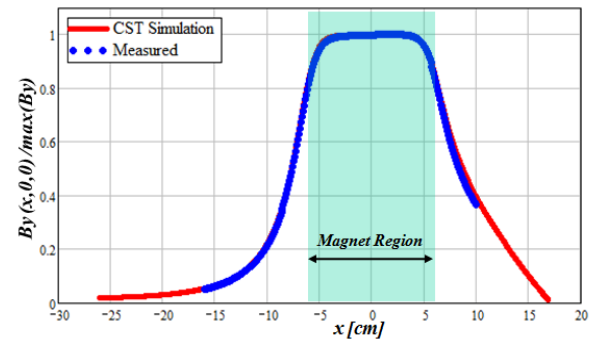


Figure 2: Dipole magnet simulated (red) and measured (blue dots) bending field distributions along the both horizontal axes.

As it can be seen, the inconsistency of the measured field is less than 2% in the magnet region and increases at far distances from magnet edges. One could also see that the

measured field amplitudes are less than expected from the simulations which are directly related to the fabrication tolerances and the yoke material properties.

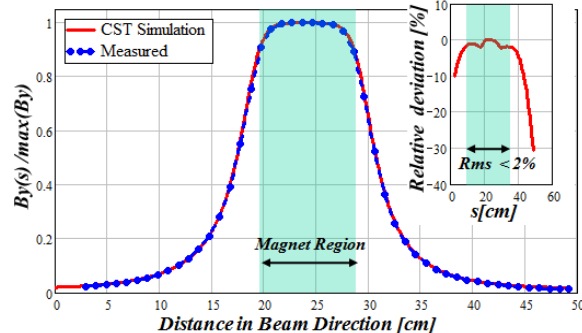


Figure 3: Dipole magnet simulated (red) and measured (blue dots) bending field distributions along the electron 90° bend trajectory (left) and measured field consistency with simulation results (right).

The final analysis of measured and simulated magnetic field results on relation between electron beam longitudinal momentum and bending field amplitude at the pole centre given as  $P_z [MeV/c] = 0.029B_0 [mT]$ .

To obtain the dispersive properties of this dipole magnet a particle tracking simulation was performed that includes five particles with different energies with the same initial position (fig. 4). In the simulation the particles energies are taken with  $\pm 0.25\text{MeV}$  and  $\pm 0.5\text{MeV}$  deviations from the design (central) particle energy of 5MeV.

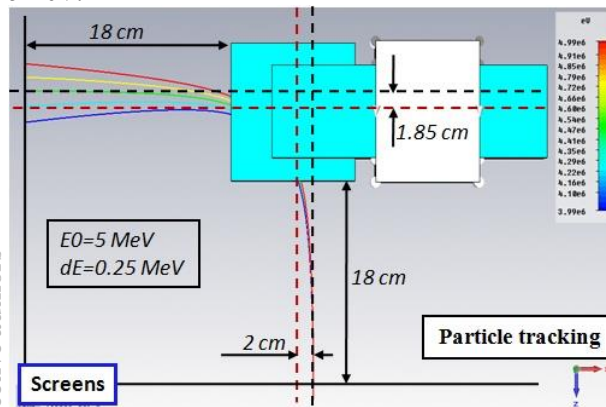


Figure 4: Trajectories of the particles with different energies passing thru the 90° bend dipole. Magnet symmetry axis (red dashed), particle design axis (black dashed) and positions of the screens are presented.

The final analysis of the transverse phase space at 18cm distance from magnet edge results on dispersion function of  $D = 0.24m$  and dispersion slope  $D' = 0.96\text{rad}$ .

Figure 5 presents the measured hysteresis curve of the dipole for maximum coil current of  $\pm 8\text{A}$ . The residual field of the magnet is  $\pm 2\text{mT}$  that is about 50 times bigger than the measured earth magnetic field of  $\sim 0.04\text{mT}$ .

Finally, magnet degauss procedure was obtained from the measurement that will be performed in three steps.

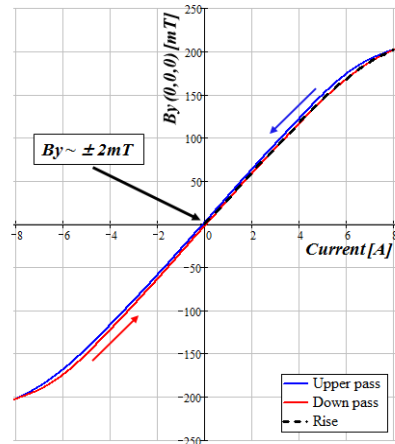


Figure 5: Measured hysteresis curve of the dipole magnet.

Finally magnet degauss procedure was obtained from measurement that will be performed by three steps.

## SOLENOID MAGNET

The AREAL solenoid magnet design (fig. 6) is the modification of the DESY solenoid. The magnet consists of single coil with 20 windings and 1 cm thick iron shielding. The magnet length is about 6.4 cm that has cooling passes in outer surfaces of the iron shield. The magnetic iron cover of solenoid provides return path for magnetic field screening effectively the field in the outer space and concentrating it inside solenoid gap.

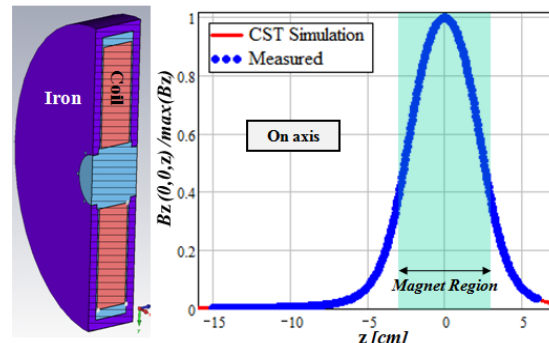


Figure 6: Solenoid magnet design (left) and on axis measured (blue dots) and simulated (red) longitudinal field profiles (right).

During the field measurements the magnet shows stable operation in term heating for the currents up the 8A that corresponds to the peak magnetic field of  $\sim 175\text{mT}$ . The figures 6 and 7 are presenting the measured and simulated focusing magnetic field longitudinal and vertical profiles. The inconsistency between measured and simulated fields is less than 2%. During the field measurements magnet-probe alignment  $<300\mu\text{m}$  was achieved.

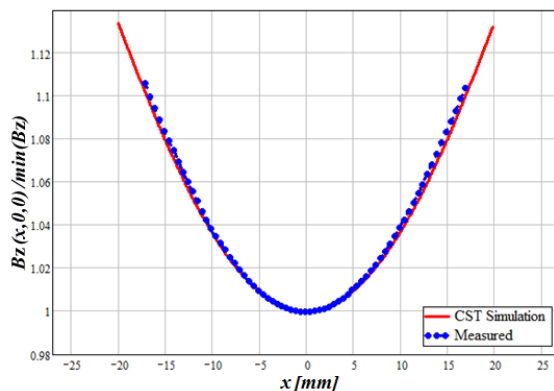


Figure 7: Solenoid magnet measured (blue dots) and simulated (red) horizontal field profiles.

The resulting field effective length of 39.57 mm was obtained that is defined as a normalized integral of  $B_z^2$ . A focal length of  $\sim 85$  cm is expected for the 5MeV electron beam at 8A solenoid current.

### “HANTEL” STEERER DESIGN

A corrector magnet (fig.8) was designed for trajectory steering of electron beams with energies up to 5MeV. The magnet is iron-free and its coils are optimized to increase homogeneous steering field region.

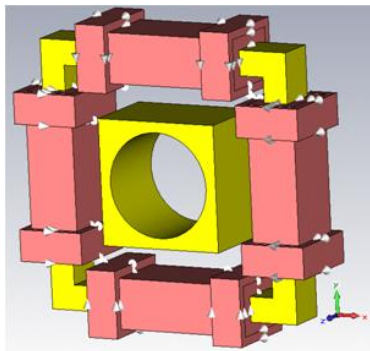


Figure 8: Iron-free steering magnet design.

The beam trajectory steering in horizontal and vertical planes will be provided by each coil doublets that are located parallel. The gap of the magnet has 50mm diameter and the maximum current of 4A is assumed in each coil doublet. Each coil consists of 480 winding in main coil and 60 windings in each edge coils. The steering field distribution is presented in Figure 10 which will provide maximum  $\sim 5.6$  mrad integrated transverse kick to the 5MeV electron beam. The effective length of the steering field is 15.2 cm and the maximum field is  $B_0 = 0.6T$  at 4A current. As it can be seen from Figure 10 the good steering field region lays within the transverse circle of radius 8mm that provides magnetic field  $<1\%$  homogeneity. From the other side, the field has none vanishing quadrupole component (fig. 11) which integrated effect in comparison with dipole component is

$<0.6\%$ . Finally, one concludes that this iron-free corrector will provide steering field with accuracy  $<1\%$  within good field region that lays in the circle of 8mm radius. The upcoming field measurements are foreseen.

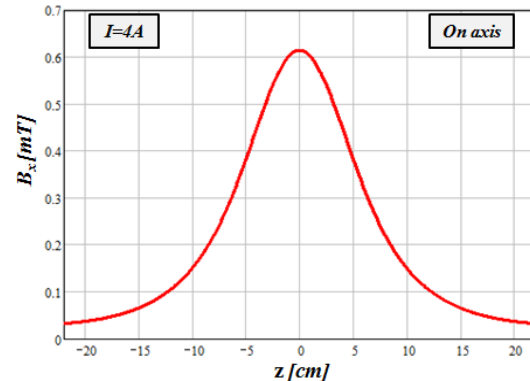


Figure 9: The steering magnetic field distribution on the magnet axis.

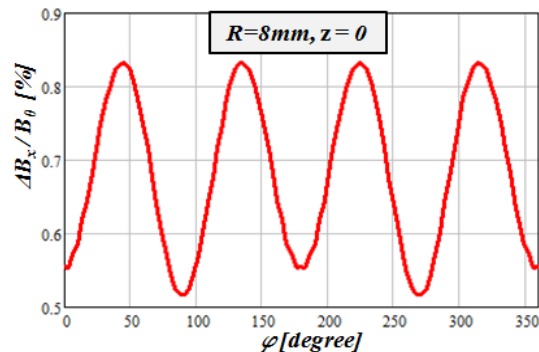


Figure 10: The angular distribution of steering magnetic field relative deviation on  $R=8$  mm circle at the centre of the magnet.

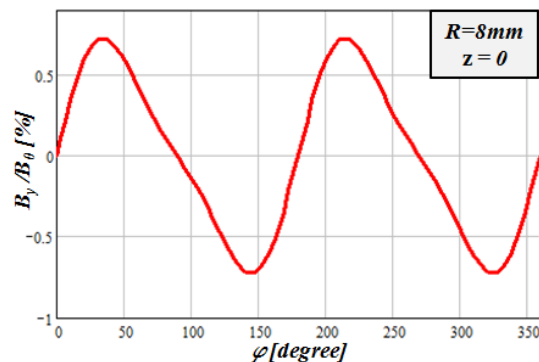


Figure 11: The angular distribution of vertical magnetic field component relative to the steering field amplitude.

### REFERENCES

- [1] B. Grigoryan et al., MOPRI017, Proc. IPAC2014, <http://jacow.org/>.
- [2] CST Studio Suite, <http://www.cst.com>